Journal of Materials Chemistry A

Accepted Manuscript

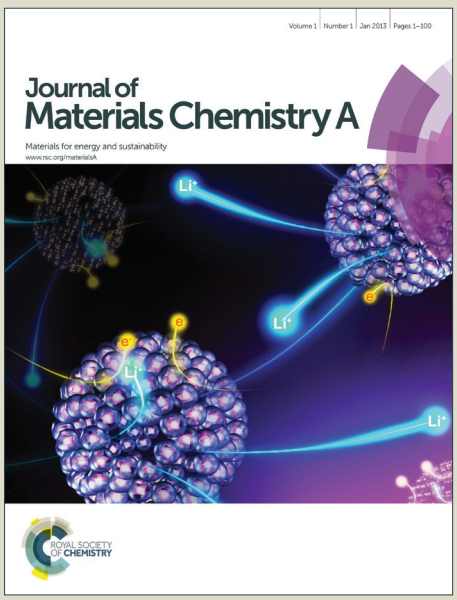

ROYAL SOCIETY OF CHEMISTRY

www.rsc.org/materialsA

Journal Name

RSCPublishing

ARTICLE

A Simple and Efficient Strategy for Chemically Tailored g-C_3N_4 Material

Cite this: DOI: 10.1039/x0xx00000x

Xiaojuan Bai,[ab] Shicheng Yan, [c] Jiajia Wang,[c] Li Wang,[a] Wenjun Jiang,[a] Songling Wu,[b] Changpo Sun, [b] Yongfa Zhu[a]*

Received 00th January 2012,
Accepted 00th January 2012

DOI: 10.1039/x0xx00000x

www.rsc.org/

Tailored nanostructures offer a new way for achieving this goal by facilitating electron-hole separation and additional opportunities to generate unique photocatalysts that demonstrated novel light absorption, thermodynamic and kinetic properties. A simple and efficient approach to the synthesis of a large variety of g-C_3N_4 tailored nanostructures was reported. Herein, NH_3 and H_2O_2 were used as controllable chemical scissor to tailor bulk g-C_3N_4 to a large variety of g-C_3N_4 nanostructures, these include exfoliated porous, quantum dot, nanomites and nanospindle. The tailored g-C_3N_4 shows a photoreactivity of H_2 evolution 3.0 (pure water) and 4.1 (saturated KCl solution) times higher than bulk g-C_3N_4 under $\lambda > 420$ nm, respectively. We believe this strategy affords new opportunities for structure tuning of *X*-doped (*X* = N, S, P, O) carbon materials, as well as their exploration in catalysis, organic synthesis, nanomedicine and energy storage.

Introduction

Research on graphite carbon nitride (g-C_3N_4) and related nanostructures has seen an enormous increase in the level of interest in recent years.[1] Nanostructured g-C_3N_4 are an appealing class of nanomaterials to complement carbon in a variety of applications. g-C_3N_4 with different structures possess not only intriguing properties including high hardness, low friction coefficient, and reliable chemical inertness, but also a great potential for energy conversion and storage, and environmental applications. [2,3]Although the electronic and optical properties of bulk g-C_3N_4 are unique and potentially useful in future devices, there is currently no easily applied method for large-scale processing of tailored nanostructured g-C_3N_4 and related objects such as nanoporous sheets, quantum dots or other nano-g-C_3N_4.[1] According to the superiority of porous graphene and carbon quantum dots when compared with conventional inorganic quantum dots and other carbon materials,[4-10] as well as the inherent unique properties of bulk g-C_3N_4 material, the tailored g-C_3N_4 nanostructures are expected to have attractive properties and so caused excellent performances in many applications.[10,11] In this sense, an macroscopic and effective method that can produce uniform tailored g-C_3N_4 with tunable size on a large scale is in great need. However, papers on the preparation of tailored g-C_3N_4 are limited, and further study on property and performances are more seldom reported. In most of the previously reported g-C_3N_4 nanostructures, various structures and morphologies of g-C_3N_4 have been produced by pyrolysis of nitrogen-rich precursors to incorporate s-triazine rings or to generate them during synthesis, and templating method.[12-16] Although good quality, nanoporous, nanosheets or nanospheres of g-C_3N_4 can be grown by this way, these approaches cannot easily be implemented for a series of various small-sized products in large-scale due to the intrinsic technological difficulties. Recently, Sadhukhan *et al.* reported microwave assisted bottom-up fabrication of g-C_3N_4 quantum dots from formamide ($HCONH_2$), and the quantum dots were produced as an intermedium, which have a nonuniform thickness ranging from 0.5 to 2.5 nm and their width ranges from 5 nm to 20 nm.[17] A convenient on-surface synthesis route would thus be a powerful alternative for the bottom-up creation of g-C_3N_4 nanostructures.

Tailored method, which was found to induce the formation of the ordered morphologies,[18-19] is a promising new method for such anisotropic chain- or stripe-like structures in the polymer matrix. Although a great number of investigations have been carried out on the formation of shear-induced patterns, this technique was rarely used in the material sciences because

these shear-induced patterns were in a metastable state. Once the shear field is changed or removed, so does the shear-induced patterns.[20] Unlike the previous reports, in this work, NH_3 and H_2O_2 were used as controllable chemical scissor for tailored g-C_3N_4 are easier and stable to process due to a lower evaporation temperature and surface functional group resulting from a significantly reduced π-π stacking, making them ideal candidates for the bottom-up production of tailored g-C_3N_4 nanostructures. Being functional materials, grain size, surface area, surface chemistry, and crystallinity are of importance to performances. *i.e.* the adsorption and active sites in catalyst are generally related with dangling bonds, surface groups, and surface electron configuration, all the above factors are related with synthesis process.[21,22] Using tunable tailored oxidation, graphene sheets can be easily stripped from graphite or nanotube, and can be further tailored into porous sheets or quantum dots.[20,23]

Based on above analysis, herein, NH_3 and H_2O_2 were used as controllable chemical scissor that tunable for g-C_3N_4 materials will be effective for further structure tailoring. The tailored method using NH_3 and H_2O_2 as the chemical scissor and the g-C_3N_4 nanostructures can be reasonably controlled by tuning NH_3/H_2O_2 stoichiometric proportion. The facile solution method capable of large scale production of tailored g-C_3N_4 is developed based on selectively cleaving -NH- between C_3N_3 and C_6N_7 in g-C_3N_4 layers. This technique is readily scalable and conceptually different from those reported for preparing g-C_3N_4 nanostructures. The tailored g-C_3N_4 present the superior photocatalytic performances and uniformly distributed sizes and can be stably dispersed in aqueous media, which can be attribtuted to the high efficiency of electron-hole separation and nanometer size effect of tailored g-C_3N_4.

Experimental section

Synthesis of Tailored g-C_3N_4 Samples

bulk g-C_3N_4: The bulk g-C_3N_4 photocatalysts were synthesized as described in a previous paper.[2] Dicyandiamide (3g) (Aldrich, 99%) in an open crucible was heated in static air with a ramping rate of 2.3°C/min to 550°C where it was held for 4 h. The product was collected and ground into powder in an agate mortar for further characterization and performance measurements. It should be claimed that the widely used "g-C_3N_4" in the literature is actually nonstoichiometric. Here we use "g-C_3N_4" to describe the products just to keep consistent with the general usage.

Tailored g-C_3N_4: The tailored g-C_3N_4 were obtained by controllable tailored of as-prepared bulk g-C_3N_4 in NH_3 and H_2O_2 aqueous solution. Typically, 50 mg of bulk g-C_3N_4 powder was dispersed in 100 mL H_2O_2 aqueous solution, and then ultrasonically dispersed for about 3 hours and afterwards the resulted suspension was stirred for another 15 h. The suspension was then centrifuged at 1000 rmp to remove the residual precipitation. Subsequently, excess NH_3 was added in the above suspension and stirred at 70 °C for a certain time. At last, the final suspension was washed several times with deionized water. In addition, NH_3/H_2O_2 ratio is one of the key for tuning tailored g-C_3N_4 nanostructures formation.

Characterization

Transmission electron microscopy (TEM) images were obtained by JEOL JEM-2011F field emission transmission electron microscope with an accelerating voltage of 200 kV. Atomic force microscopy (AFM) images were measured by SPM-9700 scanning probe microscope (Shimadzu Corporation). X-ray diffraction (XRD) patterns of the powders were recorded at room temperature by a Bruker D8 Advance X-ray diffractometer. The UV-vis absorption spectra of the suspension were recorded in the range from 200 to 800 nm using a Hitachi U-3010 spectroscope. Fourier transform infrared (FTIR) spectra were carried out using Perkin-Elmer spectrometer in the frequency range of 4000-450 cm^{-1} with a resolution of 4 cm^{-1}. The Brunauer-Emmett-Teller (BET) surface area measurements were performed by a micromeritics (ASAP 2010 V5.02H) surface area analyzer. The nitrogen adsorption and desorption isotherms were measured at 77 K after degassing the samples on a Sorptomatic 1900 Carlo Erba Instrument. Electrochemical and photoelectrochemical measurements were performed in a three electrode quartz cells with 0.1M Na_2SO_4 electrolyte solution. Platinum wire was used as counter and saturated calomel electrode (SCE) used as reference electrodes, respectively.

Photocatalytic Experiments

Photocatalytic tests were carried out in a Pyrex top-irradiation reaction vessel connected to a closed glass gas system. Hydrogen production was performed by dispersing 50 mg of catalyst powders in an aqueous solution (100 mL) containing triethanolamine (15 vol.%) as sacrificial electron donor. Co-catalysts Pt nanoparticles were introduced by in-situ photodeposition method, where 3 wt. % (respect to Pt) $H_2PtCl_6 .6H_2O$ was added and well distributed in the reaction solution. The reaction solution was evacuated several times to remove air completely prior to irradiation under a 300 W Xeon-lamp equipped with a 420 nm-cut-off filter. The temperature of the reaction solution was maintained at room temperature by a flow of cooling water during the reaction. The evolved gases were analyzed by gas chromatography equipped with a thermal conductive detector (TCD) and a 5Å molecular sieve column, using Nitrogen as the carrier gas.

Theoretical simulation calculation

Our calculations are based on the density functional theory (DFT), as implemented in the VASP[32,33] with projected augmented wave (PAW[34]) method. Generalized gradient approximation (GGA[35]) in the scheme of Perdew-Bueke-Ernzerhof (PBE[36]) is used for the exchange correlation functional. For C and N, the $2s^22p^2$ and $2s^22p^3$ orbital, respectively, are included as valence states. The cutoff energy is 500 eV. Geometry relaxations are performed until the

residual forces on each atom converged to be smaller than 0.03 eV/Å.

Results and Discussion

Tailored g-C_3N_4 Morphology

The variation of lateral size and morphology of g-C_3N_4 with NH_3/H_2O_2 treatment was clearly observed by TEM measurement (Figure 1).

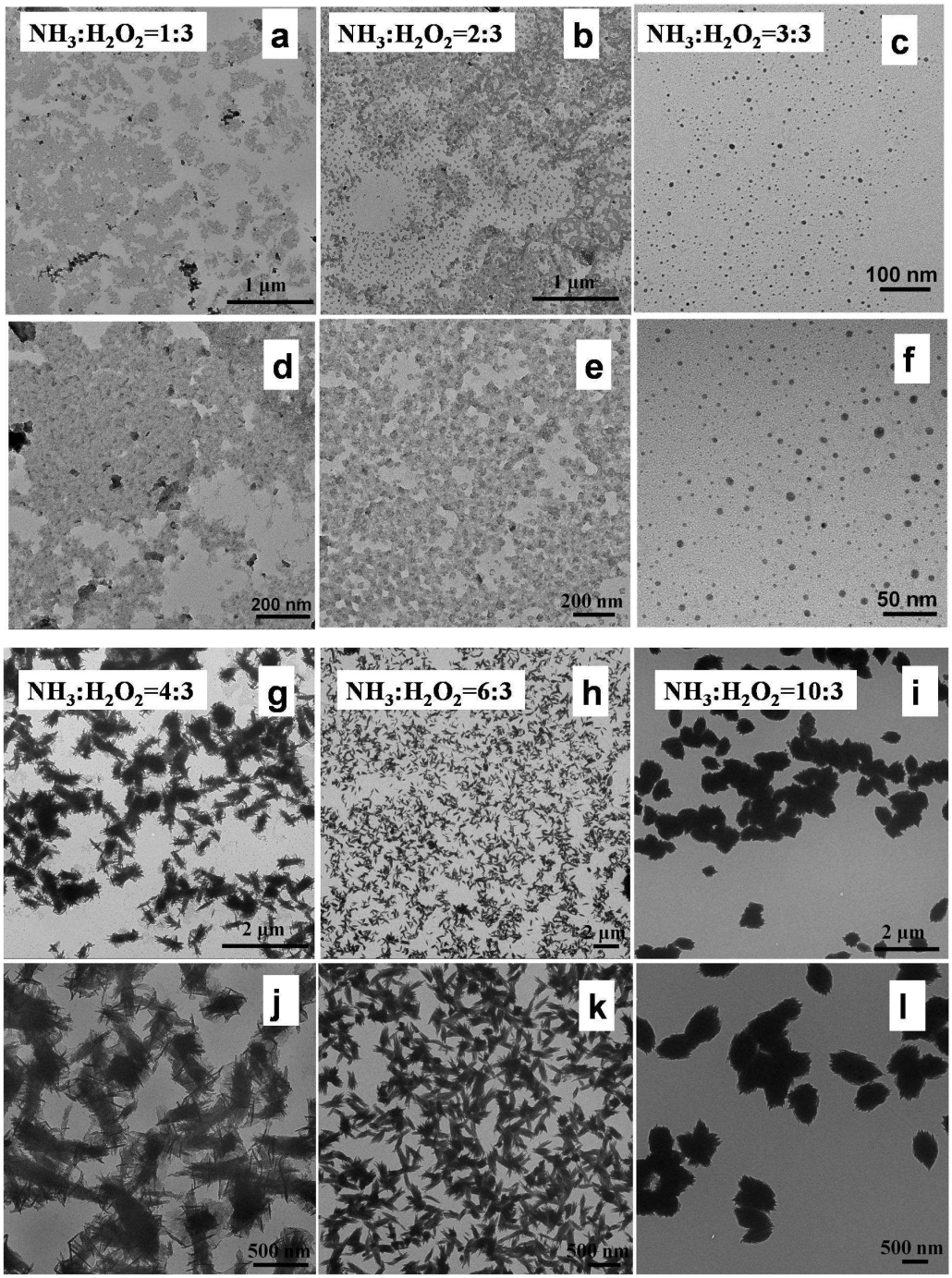

Figure 1. The evolution process of morphology for tailored g-C_3N_4. (a-l) TEM images of tailored g-C_3N_4 by treatment of different $NH_3:H_2O_2$ volume ratio (a, d) $NH_3:H_2O_2$=1:3; (b, e) $NH_3:H_2O_2$=2:3; (c, f) $NH_3:H_2O_2$=3:3; (g, j) $NH_3:H_2O_2$=4:3; (h, k) $NH_3:H_2O_2$=6:3; (i, l) $NH_3:H_2O_2$=10:3

The lateral size of bulk g-C_3N_4 prepared directly by thermal polycondensation method was relatively large and thick. The size distribution ranges widely from tens to more than two hundreds nanometers. Though the bulk g-C_3N_4 particles are

micrometers in size, they are in fact formed by closely compacted thin sheets (Figure S1). After adding "chemical scissor" NH_3/H_2O_2 mixture, the lateral size of g-C_3N_4 was decreased and became uniform more and more with increasing the concentration of NH_3/H_2O_2 (Figure 1a and d). At NH_3/H_2O_2 = 2:3, the pore size distribution of g-C_3N_4 is around 15-25 nm (Figure 1b and e). Less than 3 % g-C_3N_4 is over 30 nm. With increasing the volume ratio of NH_3/H_2O_2 to 3:3, 4:3, 6:3 and 10:3, the size distribution varied to 10-15 nm, 100-200 nm, 50-100 nm, and 400-500 nm, respectively (Figure 1c and f, g and j, h and k, i and l). After tailoring at NH_3/H_2O_2 = 2:3, the surface starts to appear pores that are uniformly distributed in g-C_3N_4 nanosheets. By further increasing the tailor time, the small pores began to cleave to form the well-ordered quantum dots until they finally form nanomites and then nanospindle.

As shown in Figure 2, the lateral size of a uniform thickness was calculated to be 2.5 nm and 0.7 nm according to the height profile along AB and CD, corresponding to g-C_3N_4 nanoporous sheets for about 7 layers (Figure 2a, b and c) and quantum dots for 2 layers (Figure 2e and g), respectively. The tailored g-C_3N_4 morphology strongly depends on the ratio of NH_3/H_2O_2, which determines the tailored degree. The g-C_3N_4 nanoporous sheets are formed with micrometer size in large under mild oxidation, the average pore size is 20 nm and the pores are uniformly distributed over g-C_3N_4 sheets. The narrow pore-size distribution indicates a large number of pores are around 4 and 15 nm (Figure 2d). Its Brunauer-Emmett-Teller (BET) specific surface area (S_{BET}) is calculated to be as high as 14.2 m^2 g^{-1}. It is about 1.6 times as large as that of bulk g-C_3N_4 (8.5 m^2 g^{-1}) but less than the theoretical value. The tightly packing nature of tailored g-C_3N_4 may be responsible for the difference between theoretical and test values. The large total pore volume strongly supports the fact that the as-prepared samples are highly nanoporous. The width of g-C_3N_4 quantum dots is 10 nm to 15 nm under deep oxidation. Thus, the nearly transparent feature of tailored g-C_3N_4 in aqueous media indicates its ultra-small size (Figure S2). The tailored g-C_3N_4 were negatively charged, with zeta potentials of about -47.1 mV and -52.1 mV (Figure S3 and S4) respectively. Benefiting from the size and charged surface, [24] the solutions are very stable, without detectable aggregation after standing for even more than two weeks. As shown in Figure 2f, the tailored method is also effective in graphene pore formation.

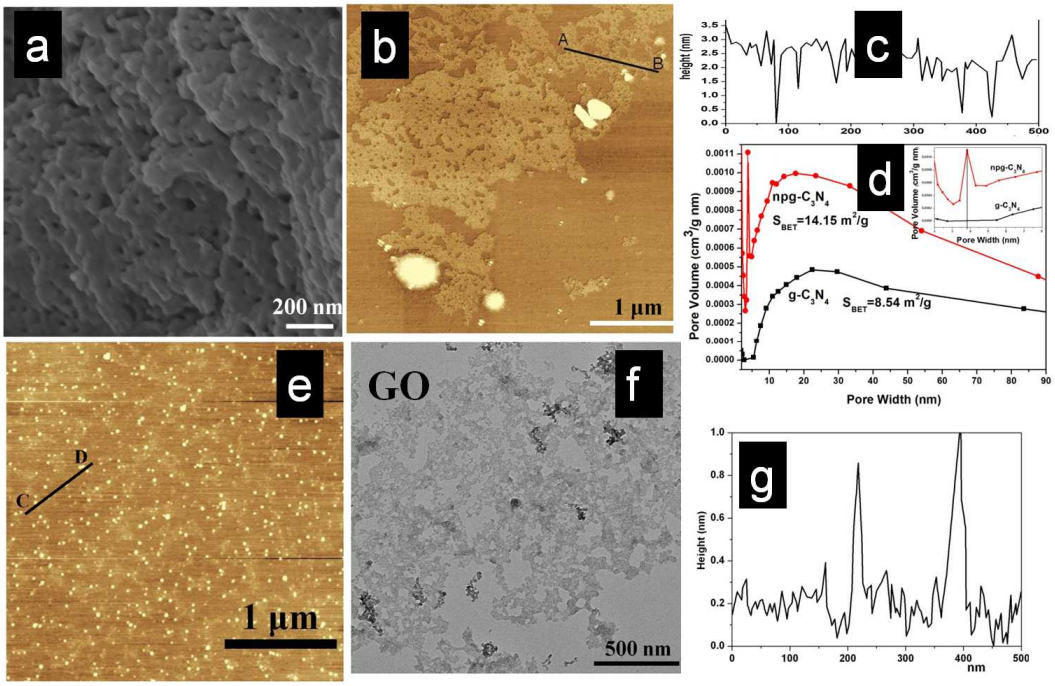

Figure 2. TEM and AFM images of tailored g-C_3N_4 nanoporous sheets (a-d) and quantum dots (e-g). (a) TEM image of g-C_3N_4 nanoporous sheets (CNPSs); (b) AFM image of CNPSs; (c) The corresponding height along AB of CNPSs; (d) Pore size distribution of bulk g-C_3N_4 and CNPSs; (e) AFM image of g-C_3N_4 quantum dots (CNQDs); (f) TEM image of tailored graphene oxide; (g) The corresponding height along CD of CNQDs.

Photocatalytic Activity and Tailored Structure

The actual photocatalytic activity of the tailored g-C_3N_4 prepared at NH_3/H_2O_2 = 2:3 for hydrogen evolution under visible light was measured in a water/triethanolamine solution in the presence of 3 wt% Pt as cocatalyst. As presented in Figure 3a, after 8 hours, the average hydrogen evolution

amount of the g-C_3N_4 nanosheets is 46 μmol, which is 3 times higher than that of bulk g-C_3N_4 (16 μmol). The hydrogen production rate can be further increased to 66 μmol, a record rate for the carbon nitride materials, being 4.1 times higher than bulk g-C_3N_4 by using a saturated salt solution of KCl to increase the active sites for hydrogen production. Electrochemical impedance spectroscopy (Figure 3b) studying the charge-transfer rate discloses the expected semicircular Nyquist plots for both tailored g-C_3N_4 and bulk g-C_3N_4, but with a significantly decreased diameter for the former. This suggests that the former owns a more effective separation of photogenerated electron-hole pairs and faster interfacial charge transfer, thus comes with a significantly increased photoreactivity.[25] The crystal and chemical structure of the g-C_3N_4 nanosheets were analyzed by diffuse reflectance absorption spectra (DRS),

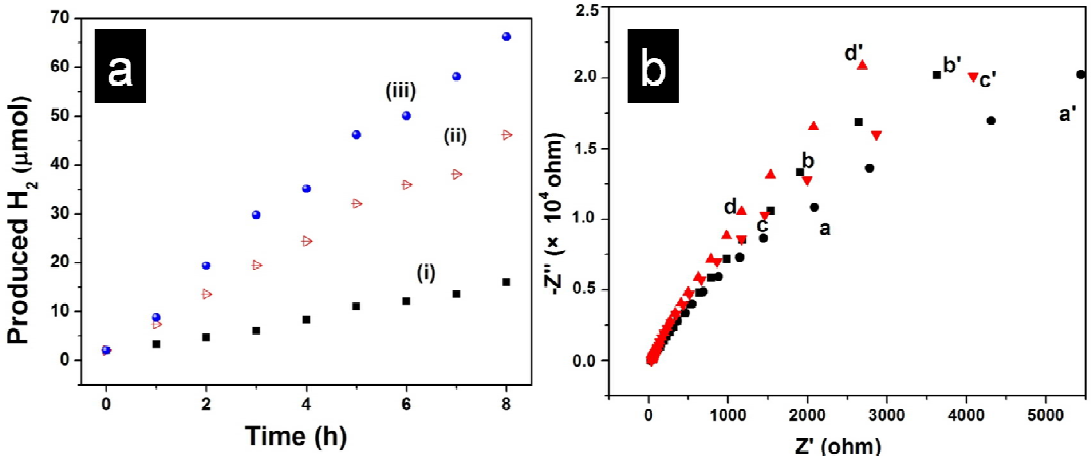

Figure 3. (a) A typical time course of H_2 production under visible light (λ > 420 nm) over 3.0 wt% Pt-deposited tailored CNPSs photocatalyst. (i) bulk g-C_3N_4 in water containing 15 vol% triethanolamine; (ii) CNPSs in water containing 15 vol% triethanolamine, (iii) CNPSs in saturated aqueous solution of KCl containing 15 vol% triethanolamine. (b) EIS Nynquist plots of CNPSs (a, a': light on; b, b': dark) and bulk g-C_3N_4 (c, c': light on; d, d': dark) with light on/off cycles under visible light ([Na_2SO_4 = 0.1 M], λ > 420 nm).

X-ray photoelectron spectra (XPS) and X-ray diffraction (XRD) patterns. DRS of bulk g-C_3N_4 and tailored g-C_3N_4 was performed and as shown in Figure S5, there is not too obvious change in the absorption edge, compared to of bulk g-C_3N_4 powder. The absorption edge in the reflectance spectra at approximately 459 nm suggests that the energy band gap of tailored g-C_3N_4 samples is similar with bulk g-C_3N_4. When the particle size reaches a certain degree, the band structure will be changed. In this work, the size of g-C_3N_4 is not enough to change the band structure. Therefore, the tailored g-C_3N_4 samples exhibit similar light absorption profile as the bulk g-C_3N_4.

To further probe the chemical state of nitrogen in the resulting g-C_3N_4 nanosheets, we conducted the XPS measurements. As shown in Figure 4, the high resolution N1s spectra can be also deconvoluted into three different peaks at binding energies of ≈400.2 (N1), 398.5 (N2) and 404.2 eV (N3), respectively. The dominant N1 is commonly attributed to sp^2 N atoms involved in triazine rings, while the medium N2 is assigned to bridging N atoms in N-(C)3 or N bonded with H atoms. The very weak N3 can be assigned to the charging effects or positive charge localization in heterocycles and the cyano-group.[26-29] The decreased intensity of N2 shows the less bridging N atoms exist in N-(C)3 or N bonded with H atoms after tailored treatment. The disappeared N3 peak for tailored g-C_3N_4 may indicate more negative charge is introduced by surface hydroxyl group during the tailored process. The result indicated that the -NH-/-NH_2 group decrease due to cleaving of chemical bond -NH- between C_3N_3 and C_6N_7.

The X-ray diffraction (XRD) patt ern of the tailored g-C_3N_4 sample shows decrease in intensity for line (002) (Figure S6), indicating that the tailored g-C_3N_4 tend to be assembled by xy-plane are in a good z-orientation compared with the bulk g-C_3N_4 powders.[24] Remarkably enough, after tailoring, the intensity of this (002) peak significantly decreases, clearly demonstrating that the layered g-C_3N_4 has been successfully tailored as we expected. This is consistent with the observations from TEM and AFM images. The appearance of new peaks for tailored g-C_3N_4 compared to bulk g-C_3N_4 is strong evidence for the creation of a new arrangement. Evidence for an in-plane pattern is shown in the well-resolved peaks at 19.24 and 23.8°, which can be indexed as (110), and (200) of the in-planar packing, respectively.[30] The other tiny peaks could be attributed to the surface microstructure of tailored g-C_3N_4, the assumption can be demonstrated by theoretical calculation.[31-36] Carbon nitride (g-C_3N_4) network materials have been produced as disordered structures by precursor-based methods, which may contain two main construction isomers-triazine and heptazine units, not an ideal structure. And the proportion of them strongly depends on the precursors and condensation process during synthesis.[31]

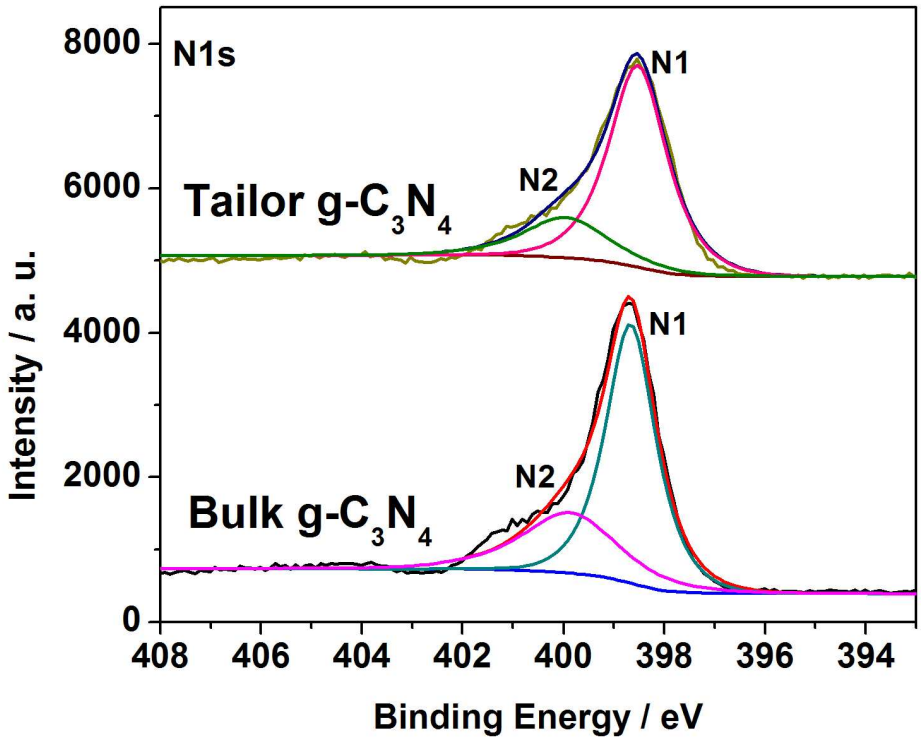

Figure 4. High-resolution XPS N1s spectra of bulk g-C_3N_4 and tailored g-C_3N_4.

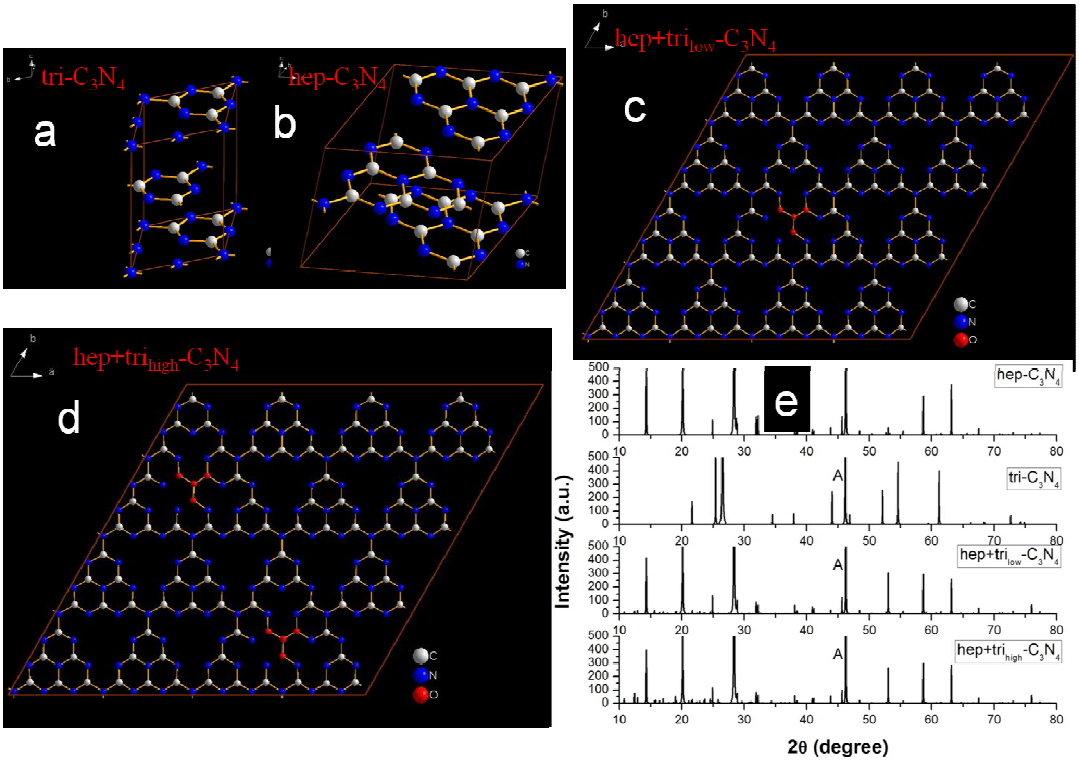

Figure 5. Calculated XRD pattern based on supercell of tri-C_3N_4 and hep-C_3N_4 (a) supercell of tri-C_3N_4; (b) supercell of hep-C_3N_4; (c) low concentrions of tri-C_3N_4 in hep-C_3N_4; (d) high concentrions of tri-C_3N_4 in hep-C_3N_4; (f) Calculated XRD pattern based on C_3N_4 of above structural unit.

Table 1 Formation energies (E^f) of hep-C_3N_4, tri-C_3N_4, hep+tri$_{low}$-C_3N_4 and hep+tri$_{high}$-C_3N_4.

Sructures	E^f (eV)
hep-C_3N_4	128.3
tri-C_3N_4	154.9
hep+tri$_{low}$-C_3N_4	145.6
hep+tri$_{high}$-C_3N_4	156.7

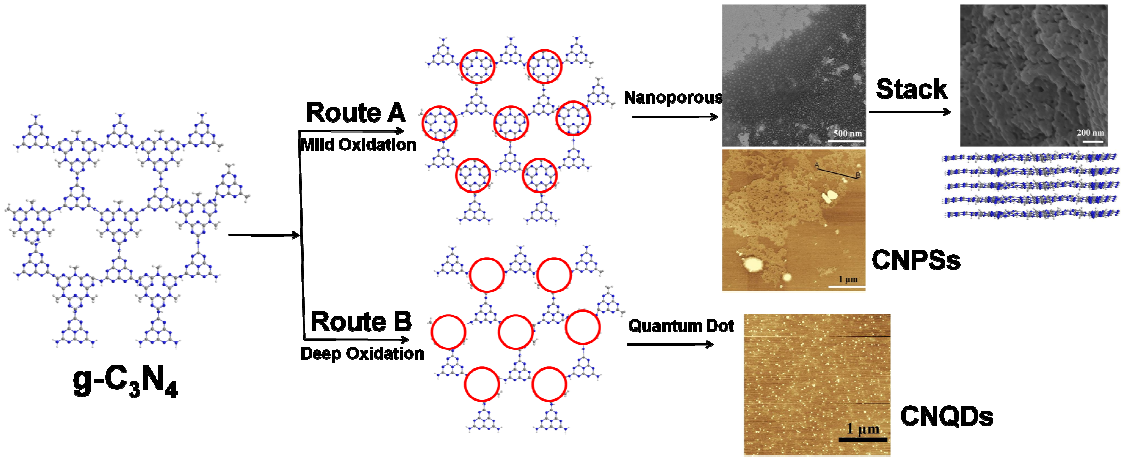

Scheme 1. Schematic illustration of tailored process from bulk g-C_3N_4 to two typical tailored morphology (CNPSs and CNQDs) by treatment of different NH_3/H_2O_2 volume ratio.

The triazine and heptazine based on C_3N_4 are shown in Figure 5a and 5b, and denoted as tri-C_3N_4 and hep-C_3N_4, respectively. To simulate the combination of tri-C_3N_4 and hep-C_3N_4, we construct a 4×4×1 supercell of hep-C_3N_4 which constains 192C and 256N atoms. Then, based on this supercell, the hep+tri$_{low}$-C_3N_4 (Figure 5c) and hep+tri$_{high}$-C_3N_4 (Figure 5d), are constructed, which correspond to the low and high concentrions of tri-C_3N_4 in hep-C_3N_4, resepctively. The theoretical X-ray diffraction (XRD) patterns are simulated using PowderCell[37] program package. Parameters used for simulation are Bragg-Branteno geometry and CuKα radiation. The XRD patterns of hep-C_3N_4, tri-C_3N_4, hep+tri$_{low}$-C_3N_4 and hep+tri$_{high}$-C_3N_4 are shown in Figure 5e, respectively. It is seen that there were more significant peaks for surface microstructure with more C_3N_3 units. As demonstrated by XRD experimental result, surface microstructure is not be observed in bulk g-C_3N_4, which is attributed that there may contains more C_6N_7 units. After tailoring, the amount of C_6N_7 units become less, this means that, the increasement of C_3N_3 units is the major cause for the appearance of surface microstructure.

To compare the stability among different g-C_3N_4 structures, the formation energy is calculated using the following relation:

$$E^f = E^t - n_C\mu_C - n_N\mu_N$$

Where E^t is the total energy of different C_3N_4 structures, μ_i (i=C, N) is the chemical potential of constituent i referenced to elemental solid/gas, and n_i is the number of ion i. In this study, μ_i (i=C, N) is simply using energy per atom in their corresponding elemental phases. According to this definition, the smaller the formation energy is, the more stable the structure will be. The formation energies of the hep-C_3N_4, tri-C_3N_4, hep+tri$_{low}$-C_3N_4 and hep+tri$_{high}$-C_3N_4 are listed in Table 1. It is seen that, (a) the hep-C_3N_4 is the most stable structure, agreeing well with other work.[38] (b) The formation energy of hep+tri$_{low}$-C_3N_4 is larger than that of hep-C_3N_4 but smaller than that of the tri-C_3N_4. This means that, when the concentration of tri-C_3N_4 in hep-C_3N_4 is low, the combination of tri-C_3N_4 and hep-C_3N_4 is one proper thermodynamically stable structure. (c) However, the formation energy of hep+tri$_{high}$-C_3N_4 is larger than that of hep-C_3N_4 and tri-C_3N_4, suggesting that the hep-C_3N_4 with high concentration of tri-C_3N_4 is thermodynamically unstable.

Proposed Tailored Mechanism

Based on the above analysis, there are two types of structural isomers in g-C_3N_4 materials, triazines (C_3N_3) and heptazines (C_6N_7), and the proportion of them strongly depends on the precursors and condensation process during synthesis.[31] The heptazines unit is energetically more stable than the triazines unit, due to the different electronic environment of nitrogen atoms. Besides, it is reported that the vacancy-free direct analogue of graphite is energetically unstable.[39] In this work, dicyandiamide ($C_2H_4N_4$), a triazine-based compound, is used to synthesize the bulk g-C_3N_4 rapidly. However, it was shown that the bulk reaction can hardly result in an ideal

composition of g-C_3N_4 material due to incomplete condensation or pyrolysis of $C_2H_4N_4$. It is known that the electronic band structure and band gap, which are very important for function of g-C_3N_4, depend on the condensation degree. It is underlined that g-C_3N_4 is functionally not only a semiconductor but also a solid state organic reagent with its surface-terminating amino groups and lone-pair N heteroatoms of the poly(tri-s-triazine) framework.[39] For example, bulk g-C_3N_4 solids perform rather poorly in some catalytic processes, while polymeric g-C_3N_4 with much disorder structure exhibits desirable activity. Structural defects or surface terminations seem to play a key role in the catalytic activation. Therefore, it is valuable to cleave -NH- between C_3N_3 and C_6N_7 to obtain more disordered and complete polymerized "g- C_3N_4 structure". According to the elemental composition of g-C_3N_4 (Table S1, Figure S7), the sample has a H/C+N atomic ratio of 3/100. However, H/C+N atomic ratios for C_3N_3 and C_6N_7 are 0 and 1/15 respectively. Then, N_{C3N3}:N_{C6H7} ratio is about 3:1, indicating that one C_6N_7 unit is mostly surrounded by three C_3N_3 units. Then in a single g-C_3N_4 layer, the C_6N_7 units inlay the C_3N_3 units. Combined with the value of bond length (C-N, C=N and N-H), the size of basic structural unit for tailored g-C_3N_4 is about 5 nm, this means that, dimension of tailored g-C_3N_4 quantum dot is mainly distributed in 10-15 nm, corresponding to about 2~3 basic structural units. The calculation value is consistent with the experimental result. Based on the above analysis, the different nanostructures were formed by different tailored degree of g-C_3N_4 which consists of C_3N_3 and C_6N_7 by using NH_3 and H_2O_2 as chemical scissor. According to the tailored process,[40, 41] a possible formation mechanism for different nanostructures is proposed in Scheme 1. H_2O_2 is inclined to heterolysis in alkaline environment to form peroxide hydroxyl anion, which would give C_3N_3 terminal group to imine and subsequent oxidation of imine terminal group, and then undergoes rearrangement to give C-OH terminal group.[42] Thus, the -NH- linking groups between C_3N_3 and C_6N_7 units are broken, and the morphology of the residue varies with the tailored degree of C_3N_3 and C_6N_7 units. Specifically, g-C_3N_4 nanoporous sheets are produced when mild oxidation conducted while the quantum dots are obtained when deep oxidation proceeded. The tailored method here is simpler, safer, and cheaper than previous approaches, which generally involve various templates.

Conclusions

In conclusion, chemically tailored method is developed to be a cheap, convenient and effective approach for mass synthesis of a large variety of g-C_3N_4 nanostructures by using NH_3 and H_2O_2 as chemical scissor. It may be readily scalable to industry level on both a theoretical and a practical level and is also demonstrated to be effective in graphene pore formation. The tailored g-C_3N_4 nanostructures from bulk g-C_3N_4 precursor can be well controlled by simply regulating the ratio of NH_3/H_2O_2. Furthermore, the formation of new tailored structures improves the charge separation process, resulting in enhanced photocatalytic activity in hydrogen production. In addition to their promising application as a photocatalyst for water splitting, we anticipate that tailored g-C_3N_4 becomes attractive for various potential applications, including catalysis, energy storage, nanomedicine, sensors and environmental protections.

Acknowledgment

This work was partly supported by National Basic Research Program of China, 973 Program (2013CB632403), National High Technology Research and Development Program of China (2012AA062701) and Chinese National Science Foundation (20925725 and 21373121).

Notes and references

[a]Department of Chemistry, Beijing Key Laboratory for Analytical Methods and Instrumentation, Tsinghua University, Beijing, China 100084
[b]Academy of State Administration of Grain, No. 11 Baiwanzhuang Street, Beijing, 100037, China.
[c]Eco-Materials and Renewable Energy Research Center (ERERC), College of Engineering and Applied Sciences, Nanjing University, NO. 22, Hankou Road, Nanjing, Jiangsu 210093, P.R. China.

Electronic Supplementary Information (ESI) available: [TEM image, FTIR spectra, XRD pattern, the elemental composition result]. See DOI: 10.1039/b000000x/

1 Y. Zheng, J. Liu, J. Liang, M. Jaroniec, S. Z. Qiao, *Energy Environ. Sci.* 2012, **5**, 6717-6731.
2 X. C. Wang, K. Maeda, A. Thomas, K. Takanabe, G. Xin, J. M. Carlsson, K. Domen, M. Antonietti, *Nature Mater*. 2009, **8**, 76-80.
3 L. M. Zambov, C. Popov, N. Abedinov, M. F. Plass, W. Kulisch, T. Gotszalk, P. Grabiec, I. W. Rangelow, R. Kassing, *Adv. Mater.* 2000, **12**, 656-660.
4 S. N. Baker, G. A. Baker, *Angew. Chem., Int. Ed.* 2010, **49**, 6726-6744.
5 L. Cao, X. Wang, M. J. Meziani, F. Lu, H. Wang, P. G. Luo, Y. Lin, B. A. Harruff, L. M. Veca, D. Murray, S. Y. Xie, Y. P. Sun, *J. Am. Chem. Soc.* 2007, **129**, 11318-11319.
6 H. X. Zhao, L. Q. Liu, Z. D. Liu, Y. Wang, X. J. Zhao, C. Z. Huang, *Chem. Commun*. 2011, **47**, 2604-2606.
7 F. Wang, Y. Chen, C. Liu, D. Ma, *Chem. Commun*. 2011, **47**, 3502-3504.
8 H. Li, X. He, Z. Kang, H. Huang, Y. Liu, J. Liu, S. Lian, C. H. A. Tsang, X. Yang, S. T. Lee, *Angew. Chem., Int. Ed.* 2010, **49**, 4430-4434.
9 P. Luo, C. Li, G. Q. Shi, *Phys. Chem. Chem. Phys.* 2012, **14**, 7360-7366.
10 S. Zhu, S. Tang, J. Zhang, B. Yang, *Chem. Commun.* 2012, **48**, 4527-4539.
11 L. A. Ponomarenko, F. Schedin, M. I. Katsnelson, R. Yang, E. W. Hill, K. S. Novoselov, A. K. Geim, *Science* 2008, **320**, 356-358.
12 E. Kroke and M. Schwarz, *Coord. Chem. Rev*. 2004, **248**, 493-532.
13 A. Thomas, A. Fischer, F. Goettmann, M. Antonietti, J. O. Muller, R. Schlogl, J. M. Carlsson, *J. Mater. Chem*. 2008, **18**, 4893-4908.
14 Y. Wang, X. Wang and M. Antonietti, *Angew. Chem. Int. Ed*. 2012, **51**, 68-89.
15 Y. Wang, X. Wang, M. Antonietti, Y. Zhang, *ChemSusChem* 2010, **3**, 435-439.

16 F. Goettmann, A. Fischer, M. Antonietti, A. Thomas, *Angew. Chem. Int. Ed*. 2006, **45**, 4467-4471.
17 M. Sadhukhan, S. Barman, *J. Mater. Chem. A* 2013, **1**, 2752-2756.
18 K. B. Migler, *Phys. Rev. Lett*. 2001, **86**, 1023-1026.
19 J. A. Pathak, K. B. Migler, *Langmuir* 2003, **19**, 8667-8674.
20 C. Mao, J. R. Huang, Y. T. Zhu, W. Jiang, Q. X. Tang, X. J. Ma, *J. Phys. Chem. Lett*. 2013, **4**, 43-47.
21 Y. C. Zhao, Z. Liu, W. G. Chu, L. Song, Z. X. Zhang, D. L. Yu, Y. J. Tian, S. S. Xie, L. F. Sun, *Adv. Mater*. 2008, **20**, 1777-1781.
22 Y. Wang, J. S. Zhang, X. C. Wang, M. Antonietti, H. R. Li, *Angew. Chem., Int. Ed*. 2010, **49**, 3356-3359.
23 D. Wang, L. Wang, X. Y. Dong, Z. Shi, J. Jin, *Carbon* 2012, **50**, 2147-2154.
24 X. Zhang, X. Xie, H. Wang, J. Zhang, B. Pan, Y. Xie, *J. Am. Chem. Soc*. 2013, **135**,18-21.
25 H. L. Guo, X. F. Wang, Q. Y. Qian, F. B. Wang, X. H. Xia, *ACS Nano* 2009, **3**, 2653-2659.
26 A. Vinu, *Adv. Funct. Mater*. 2008, **18**, 816-827.
27 Y. G. Li, J. A. Zhang, Q. S. Wang, Y. X. Jin, D. H. Huang, Q. L. Cui, G. T. Zou, *J. Phys. Chem. B* 2010, **114**, 9429-9434.
28 R. C. Dante, P. Martin-Ramos, A. Correa-Guimaraes, J. Martin-Gil, *Mater. Chem. Phys*. 2011, **130**, 1094-1102.
29 Y. J. Cui, J. S. Zhang, G. G. Zhang, J. H. Huang, P. Liu, M. Antonietti, X. C. Wang, *J. Mater. Chem*. 2011, **21**, 13032-13039.
30 M. Shalom, S. Inal, C. Fettkenhauer, D. Neher, M. Antonietti, *J. Am. Chem. Soc*. 2013, **135**, 7118-7121.
31 M. Deifallah, P. F. McMillan, F. Cora, *J. Phys. Chem. C* 2008, **112**, 5447-5453.
32 G. Kresse, J. Furthmiiller, *Computational Materials Science* 1996, **6**, 15-50
33 G. Kresse, J. Hafner, *Physical Review B*. 1993, **47**, 558-561.
34 P. E. Blochl, *Physical Review B*. 1994, **50**, 953-979.
35 J. P. Perdew, J. A. Chevary, S. H. Vosko, K. A. Jackson, M. R. Pederson, D. J. Singh, C. Fiolhais, *Physical Review B*. 1992, **46**, 6671-6687.
36 J. P. Perdew, K. Burke, M. Ernzerhof, *Physical Review Letters*. 1996, **77**, 3865-3868.
37 W. Kraus, G. Nolze. Computer Programs. *J. Appl. Cryst.* 1996, **29**, 301-303.
38 E. Kroke, M. Schwarz, E. Horath-Bordon, P. Kroll, B. Noll, A. D. Norman. *New J. Chem*. 2002, **26**, 508-512.
39 F. Z. Su, S. C. Mathew, G. Lipner, X. Z. Fu, M. Antonietti, S. Blechert, X. C. Wang, *J. Am. Chem. Soc*. 2010, **132**, 16299-16301.
40 K. Suzuki, T. Watanabe, S. I. Murahashi, *J. Org. Chem.* 2013, **78**, 2301-2310.
41 M. T. Schümperli, C. Hammond, I. Hermans, *ACS Catal*. 2012, **2,** 1108-1117.
42 M. T. Schumperili, C. Hammond, I. Hermans, *Phys. Chem. Chem. Phys*. 2012, **14**, 11002-11007.

Graphical Abstract

Scheme Titles

Scheme 1. Schematic illustration of tailored process from bulk g-C_3N_4 to two typical tailored morphology (CNPSs and CNQDs) by treatment of different NH_3/H_2O_2 volume ratio.